Qi et al. Cell Communication and Signaling (2025) 23:168
https://doi.org/10.1186/s12964-025-02167-2

Cell Communication and Signaling

RESEARCH

Open Access

HOXC6 promotes the metastasis of MSI-H CRC by interacting with M2 macrophages and inducing effector T cell exhaustion

Lina Qi[1†], Biting Zhou[1†], Jiani Chen[1†], Kailun Xu[1], Kailai Wang[1], Shu Zheng[1], Wangxiong Hu[1,2*] and Yanmei Yang[3*]

Abstract

We previously discovered that *HOXC6* was the most significantly upregulated gene in right-sided colon cancer compared to left-sided colon cancer according to our previous study; however, the role of HOXC6 in microsatellite instability-high (MSI-H) tumors remains poorly understood. Here, multiple public datasets, and in-house cohorts were used to analyze the differential expression and prognostic role of HOXC6 in colorectal cancer (CRC). Immunohistochemistry and immunofluorescence were performed to evaluate the correlation between HOXC6 expression and M2 macrophage infiltration. CCK8 and Transwell assays were used to evaluate the proliferation and migration of tumor cells in vitro. BALB/c nude mice were utilized to construct a humanized immune system model to evaluate the efficacy of ruxolitinib in vivo. We found that HOXC6 was overexpressed in MSI-H CRC and associated with a poor prognosis. Upregulation of CCL2 by HOXC6 increased M2 macrophage infiltration. IL6 secreted by M2 macrophages induced the epithelial-mesenchymal transition of tumor cells by upregulating HOXC6. M2 macrophages promoted effector T cell exhaustion by downregulating 4-1BB. Thus, inhibition of the IL6/JAK pathway in M2 macrophages restored 4-1BB expression and T-cell cytotoxicity offering a promising therapeutic target for the treatment of HOXC6-overexpressing MSI-H CRC.

Keywords Colorectal cancer, MSI-H, 4-1BB, HOXC6, M2 macrophages

Introduction

Although immunotherapy represented by immune checkpoint blockade (ICB) has been very successful in the field of cancer treatment, the global partial response (PR) and complete response (CR) rates are less than 50%, even for microsatellite instability-high (MSI-H) colorectal cancer (CRC) [1, 2]. The high heterogeneity of MSI-H disease has been depicted in CRC and gastric cancer in our previous studies [3, 4]. Thus, it is urgent to stratify the MSI-H group into different subtypes and adopt targeted therapy to prolong patient survival. We previously found that *HOXC6* was the most significantly upregulated gene in the right-sided colon cancer (RCC) compared to the left-sided colon cancer (LCC) [5], and *HOXC6* can promote CRC metastasis by orchestrating

[†]Lina Qi, Biting Zhou and Jiani Chen contributed equally to this work.

*Correspondence:
Wangxiong Hu
wxhu@zju.edu.cn
Yanmei Yang
yangyanmei@zju.edu.cn
[1] Cancer Institute (Key Laboratory of Cancer Prevention and Intervention, National Ministry of Education), The Second Affiliated Hospital, Zhejiang University School of Medicine, Hangzhou, Zhejiang 310009, China
[2] Research Center for Air Pollution and Health, School of Medicine, Zhejiang University, Hangzhou, Zhejiang 310009, China
[3] Key Laboratory of Reproductive and Genetics, Ministry of Education, Women'S Hospital, Zhejiang University School of Medicine, Hangzhou, Zhejiang 310006, China

the Dickkopf-1 (DKK1)/Wnt/beta-catenin axis within the tumor itself. In addition, there was a significant negative correlation between HOXC6 and MLH1. MLH1 is a key protein involved in the DNA mismatch repair (MMR) pathway [6]. However, the potential relevance of HOXC6 and MSI-H CRC progression and the underlying mechanism remain unknown.

In this study, we discovered a novel association between HOXC6 and MSI-H tumor microenvironment remodeling. We first found that high HOXC6 expression was associated with a worse prognosis, even in the MSI-H CRC cohort. High expression of HOXC6 was significantly associated with M2 macrophage infiltration within the tumor microenvironment (TME). Moreover, interleukin 6 (IL6) secreted by M2 macrophages induced effector T cells inactivationby downregulating 4-1BB. Treatment of M2 macrophages with ruxolitinib (an inhibitor of the IL6/JAK pathway) restored restored 4-1BB expression in T cells and demonstrated high cytotoxicity against HCT116 cells with high HOXC6 expression. Additionally, the combination of ruxolitinib and toripalimab (an anti-PD1 antibody) enhanced the antitumor effect on tumors with high HOXC6 expression, which clarified the crosstalk between CRC, tumor associated macrophages (TAMs), and cytotoxic T cells and revealed a good candidate target in the treatment of MSI-H metastatic CRC (mCRC).

Materials and methods

Bioinformatic analysis of transcriptome datasets

All Level 3 CRC RNASeqV2 mRNA expression profiles were obtained from The Cancer Genome Atlas (TCGA, 09/26, 2019). The raw CEL files of GSE39582 (Affymetrix HG U133 Plus 2.0 arrays) were downloaded from Gene Expression Omnibus (GEO) and processed using the *affy* package of BioConductor [7]. Then, the MAS5 algorithm was used for background correction, normalization and summarization of single probes for all probe sets. The identification of differentially expressed genes (DEGs) between subgroups was performed as in our previous studies [3, 8]. Significant DEGs were selected according to a false discovery rate (FDR) adjusted P value < 0.05 and fold change > 2. Gene Ontology (GO) and Kyoto Encyclopedia of Genes and Genomes (KEGG) enrichment analyses were performed using the *clusterProfiler* package from Bioconductor based on the DEGs identified between the HOXC6 + (> median) and HOXC6- (< median) groups [9]. Significantly enriched GO terms and pathways were selected according to an FDR-adjusted P value < 0.01. Hallmark gene sets from the molecular signatures database (MSigDB) [10] were used to determine whether any signatures were enriched in specific groups by gene set enrichment analysis (GSEA) [7]. Significantly enriched hallmarks were chosen according to a P value < 0.05.

To quantify the relative abundance of distinct lymphocytes in CRC, CIBERSORT [11] was used to calculate the proportions of 22 lymphocytes in tumor tissue. The permutation was set to ≥ 100, and quantile normalization of the input expression mixture was set to FALSE for the TCGA RNAseq dataset. Samples with a P value > 0.05 were excluded from further comparisons. Consensus tumor purity was refined based on a previous systematic pancancer measurement of tumor purity [12].

Immunofluorescence (IF) staining and calculation of the CD206-positive area

A total of 53 stage II and 47 stage III&IV RCC formalin-fixed paraffin-embedding (FFPE) samples collected from Zhejiang University Cancer Institute (ZUCI) were used for IF staining to evaluate the expression of CD206 (a marker of M2 macrophages). Written informed consent was obtained from all patients before enrollment. A primary antibody against CD206 (1:200, HUABIO, ET1702-04) was used for IF staining. ImageJ was used to calculate the CD206-positive area percentage. In brief, the image was separated based on the channels and displayed as 8-bit images. Then, the threshold was adjusted. The areas of the regions stained with DAPI (4',6-diamidino-2-phenylindole, a nuclear dye) and CD206 were calculated. The percentage of CD206-positive area was calculated as (CD206-positive area)/(DAPI-positive area).

Cell culture and coculture

The HCT116 and THP-1 cell lines were purchased from American Type Culture Collection (ATCC) and cultured with RPMI 1640 medium (Gibco) containing 10% fetal bovine serum (FBS, BI Industry). The cells were incubated at 37 ℃ with 5% CO_2. M2 macrophages were generated from THP-1 cells in vitro. Briefly, THP-1 cells were first treated with 200 nM PMA (phorbol 12-myristate 13-acetate, Sigma-Aldrich, Catalog Number: P1585) for 24 h to differentiate into macrophages. Then, 20 ng/ml IL-4 (Sigma-Aldrich, Catalog Number: SRP4137) and 20 ng/ml IL-13 (PeproTech, Catalog Number: 200–13) were added for 48 h to induce M2 macrophage differentiation. $CD8^+$ T cells were isolated from peripheral blood mononuclear cells (PBMCs) and stimulated with IL2 (Sino-Biological, Catalog Number: GMP-11848-HNAE-B) and OKT3 (BD Pharmingen, Catalog Number: 566685) as described in our previous work [13].

Cocultivation of macrophages, $CD8^+$ T cells, and/or HCT116 cells was conducted with a noncontact coculture Transwell system (Corning, USA). Inserts containing 1.0×10^6 THP-1 cells or M2 macrophages were

transferred to 6-well plates previously seeded with HCT116 cells (2.5×10^5 cells per well) and cocultured in 1.5% FBS-containing medium for 72 h. HCT116, THP-1, or M2 macrophages were cultured in 1.5% FBS-containing medium as a negative control. After coculture, macrophages, $CD8^+$ T cells, HCT116 cells and culture medium were harvested for use. IL6 was purchased from PeproTech (Catalog Number: 200–06).

Stable gene overexpression using the lentiviral transfection system

LV-HOXC6 (Gene, Shanghai, 24024–1) and negative control lentivirus (CON238) were purchased from GeneChem (Shanghai, China). For infection, 1×10^5 cells were plated into 6-well plates and cocultured with 2.5×10^6 transducing-units (TU) virus in the presence of 1×HitransG (GeneChem, Shanghai, China) and standard medium. Twelve to 15 h later, the medium was replaced with fresh complete culture medium. After 72 h of transfection, 2 μg/ml puromycin was added to the culture medium for HCT116 selection. Western blotting and quantitative reverse transcription-polymerase chain reaction (qRT-PCR) were utilized to confirm HOXC6 overexpression.

siRNA knockdown

Cells were plated into 6-well plates. After the cells grew to 50–60% confluence, Lipo3000 (Invitrogen) with specific siRNA (Genepharma, Shanghai) was added to the cells according to the manufacturer's suggestions. The final concentration of siRNA was 100 nM. Cells were incubated with siRNA for 48 h and then harvested for protein and RNA extraction. The sequences of *HOXC6* siRNAs were as follows: sense: 5'-GAAAGCCAGUAUCCAGAUUTT-3' and antisense: 5'-AAUCUGGAUACUGGCUUUCTT-3'. The sequences of *IL6* siRNAs were as follows: sense: 5'-CCCAGGAGAAGAUUCCAAATT-3' and antisense: 5'-UUUGGAAUCUUCUCCUGGGTT-3'. The negative control siRNA sequences were as follows: sense: 5'-UUCUCCGAACGUGUCACGUTT-3' and antisense: 5'-ACGUGACACGUUCGGAGAATT-3'.

Transwell migration assays

Cell migration was examined by Transwell assays without Matrigel. Approximately 10^4 cells were plated into the upper chamber with RPMI 1640 medium without FBS. RPMI 1640 medium supplemented with 20% FBS was added to the lower chamber. After 48 h of culture for HCT116 cells, the cells in the upper chamber were removed, and cells under the upper chamber were fixed with 4% formalin and stained with crystal violet. The migrated cells were counted by light microscopy, and the mean cell number of three random visual fields at a magnification of 200× was recorded.

Cell proliferation

Approximately 1×10^3 cells were plated into 96-well plates. Cell viability was measured at 1, 3, 5, and 7 days after plating. Cell Counting Kit-8 (CCK-8, Dojindo, Japan, CK04) was utilized for cell viability testing. Cell culture medium was used as a blank control. After 2–3 h of incubation, an optimal density (OD) value of 450 nm was used to detect cell proliferation. Experiments were carried out in triplicate. Ruxolitinib (INCB018424) was purchased from Selleck.

Determination of the effectiveness of effector T cells to tumor cells

Effector T cells were cocultured with HCT116 cells and/or M2 macrophages for 48 h in a 96-well plate. Lactic dehydrogenase (LDH) released from tumor cells was detected using a cytotoxicity LDH detection kit (Genmed) following the manufacturer's instructions. The amount of LDH released was used to assess the lysis of target cells, which reflect the lethal effect of effector cells. Percent cytotoxicity was calculated according to OD values using the following formula:Cytotoxicity% = (Experimental-Effector spontaneous-Target spontaneous)/(Target maximum-Target spontaneous)×100%.

Protein extraction and western blotting

Radioimmunoprecipitation assay (RIPA) buffer (Beyotime) with 1% protease inhibitor cocktail (Roche Applied Science) was used for total protein extraction. After quantification of protein concentration and boiling with protein loading buffer, 10% SDS–polyacrylamide gel electrophoresis (SDS-PAGE) gels were used to separate proteins, and polyvinylidene fluoride (PVDF) membranes were used for protein transition. After blocking with 5% nonfat milk, the PVDF membranes were incubated with primary antibodies followed by horseradish peroxidase (HRP)-linked secondary antibodies. Enhanced chemiluminescence (ECL) reagent was used to detect the protein bands. The primary antibodies used for western blotting were as follows: anti-HOXC6 (Santa Cruz, sc-376330, dilution 1:1000), anti-epithelial mesenchymal transition (EMT) antibody kit (Cell Signaling Technology, #9782, dilution 1:1000), anti-IL6 (Abcam, ab233551, dilution 1:1000), and anti-β-tubulin (Huabio, Hangzhou, M1305-2, dilution 1:5000). β-Tubulin was used as a protein loading control.

DNA isolation and high-throughput sequencing

CRC and matched normal mucosa were obtained from the Second Affiliated Hospital, School of Medicine of Zhejiang University. DNA extraction, sequencing, mutation calling, and MSI-H definition of the 338 fresh frozen samples were performed as described in our previous work [14, 15].

RNA sequencing and qRT-PCR

RNA extraction and PE150 Illumina sequencing of the 99 fresh frozen ZUCI MSI-H CRC samples were performed as described in our previous work [14]. The mismatch repair status [mismatch repair deficient (dMMR) or mismatch repair proficient (pMMR)] was determined by using immunohistochemistry (IHC) detection of MLH1, PMS2, MSH2 and MSH6 expression of their corresponding FFPE sections, and the samples were subjected to blinded analysis of MSI status by three pathologists specializing in CRC at the Second Affiliated Hospital, Zhejiang University School of Medicine. Total RNA from HCT116 and $CD8^+$ T cells was extracted using TRIzol following a standard protocol. The Takara PrimeScript TM RT Master Mix Kit (Takara, RR036Q) was used for reverse transcription. iTaq Universal SYBR Green Supermix (Bio-Rad) and Applied Biosystems 7500 Fast Real-Time PCR System were applied for qRT-PCR. GAPDH was used as the loading control. Experiments were carried out in triplicate. The results were calculated as follows: $\Delta CT = CT_{Experimental/NC}\text{-}CT_{GAPDH}$, $\Delta\Delta CT = \Delta CT_{Experimental/NC}\text{-}\Delta CT_{NC}$, fold change $= 2^{-\Delta\Delta CT}$. The primers used for qRT-PCR are as follows:

	Forward sequence (5′ to 3′)	Reverse sequence (5′ to 3′)
4-1BB	TCTTCCTCACGCTCC GTTTCTC	TGGAAATCGGCAGCT ACAGCCA
CCL2	AAGATCTCAGTGCAG AGGCTCG	CACAGATCTCCTTGG CCACAA
CD163	TTTGTCAACTTGAGT CCCTTCAC	TCCCGCTACACTTGT TTTCAC
CD206	GGGTTGCTATCACTC TCTATGC	TTTCTTGTCTGTTGCCGT AGTT
CD27	TGCAGAGCCTTGTCG TTACAG	GCTCCGGTTTTCGGT AATCCT
CD28	CTATTTCCCGGACCT TCTAAGCC	GCGGGGAGTCATGTT CATGTA
CTLA4	CATGATGGGGAATGA GTTGACC	TCAGTCCTTGGATAG TGAGGTTC
HOXC6	GAGAATGTCGTGTTC AGTTC	GATCTGTCGCTCGGT CAGGCAA
IL6	CCTTCGGTCCAGTTG CTTCT	CCAGTGCCTCTTTGC TGCTTTC
LAG3	TGGCGACTTTACCCT TCGAC	AAACTCCTCTGGGAT GGGGT
PD1	CGTGGCCTATCCACT CCTCA	ATCCCTTGTCCCAGC CACTC
TIGIT	TGGTCGCGTTGACTA GAAAGA	GGGCTCCATTCCTCC TGTC
TIM3	AAGGACCTCGGCTGG AAGTGC	CCGGGTTATGCTGGT TGTA
GAPDH	ATCCCATCACCATCT TCCAG	TGAGTCCTTCCACGA TACCA

Evaluation of CCL2, IFN-γ, and TNF-α by enzyme-linked immunosorbent assay (ELISA)

Approximately 5×10^5 cells were plated into 6-well plates. After the specified treatments according to the manufacturer's suggestions, the culture medium was harvested simultaneously. Detection of secreted human CCL2, IFN-γ, and TNF-α were performed using h.MCP-1 ELISA kit (BOSTER, Wuhan, China, Lot: EK0441), IFN-γ ELISA kit (BOSTER, Wuhan, China, Lot: EK0373), and TNF-α ELISA kit (Absin, Shanghai, China, Lot: abs551818) according to the manufacturers' instructions.

In vivo imaging assays

Six- to eight-week-old female BALB/c nude mice with tail vein injection of 1×10^6 $CD8^+$ T cells and 1×10^5 M2-TAMs per mice were used to establish a simplified model with a humanized immune system, and tail vein injection of 1×10^6 Luc-HCT116-OE or Luc-HCT116-NC cells was performed to establish a metastasis model (each group has five nude mice). Mice were anesthetized with isoflurane, then intraperitoneally injected with 100 µl (3 mg) D-luciferin (Cayman, Lot: 14,681) and imaged. Drug treatment started after detection of lung metastasis, with daily oral gavage of ruxolitinib (50 mg/kg) and intraperitoneal injection of toripalimab (200 µg/mouse) for 10 consecutive days. Imaging was performed on day 41, after which the experiment was terminated and the liver and lung tissues were harvested for further experiments.

Single cell sequencing

To construct the subcutaneous tumor xenograft mouse model, 5×10^6 mice MC38 HOXC6-OE and HOXC6-NC cells were injected subcutaneously at the costal margin of six-week-old female c57BL/6 mice. The size of the xenograft tumor was measured every 3 days. The mice were killed six weeks later, and the subcutaneous xenograft tumors were dissected and weighed. Then, we randomly chose one xenograft tumor in each group for single cell transcriptome sequencing in Singleron company (China). Single cell data analysis was performed by Seurat (V 5.2.0) package in R [16].

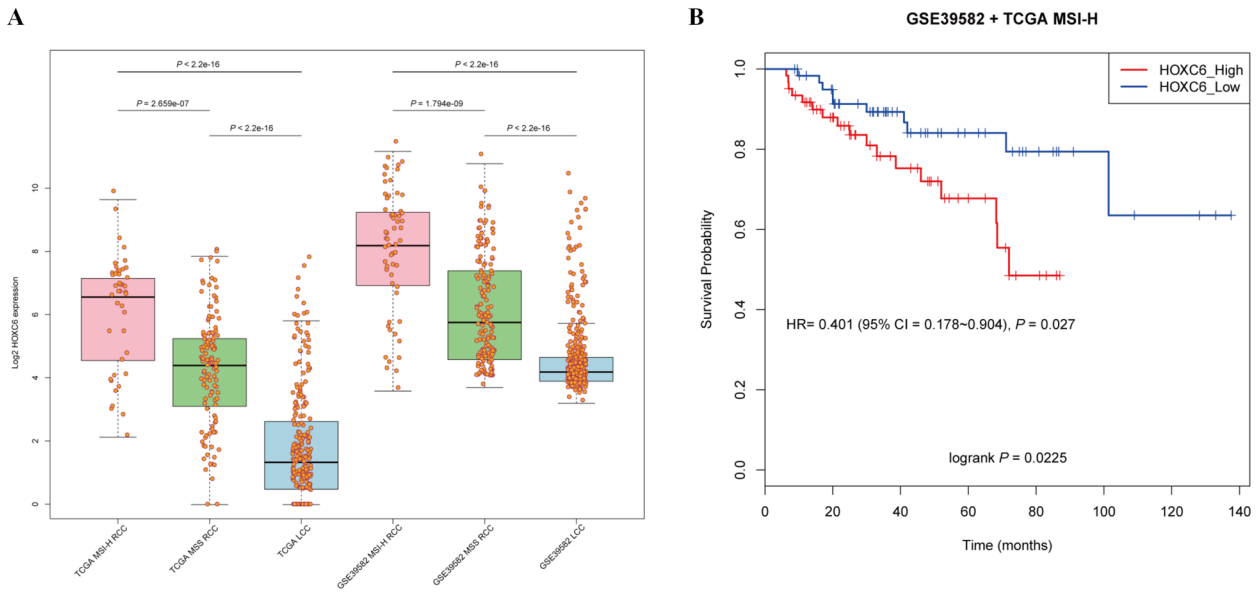

Fig. 1 Expression of HOXC6 and prognostic value in CRC. **A** HOXC6 was overexpressed in MSI-H RCC compared to MSS RCC and LCC in both the TCGA dataset and the GSE39582 dataset. **B** KM plot showing that the high HOXC6 expression group had a poorer prognosis than the low expression group in the MSI-H CRC cohort

Statistical analysis

All statistical analyses and graphical generation steps were performed in the R programming language (×64, version 3.5.1), IBM SPSS Statistics 22 and GraphPad Prism7 unless otherwise specified.

Results

HOXC6 is overexpressed in MSI-H CRC and associated with a poor prognosis

We previously revealed that HOXC6 is upregulated in RCC compared to LCC and normal colon tissues [5, 8]. Then, we further explored the expression pattern of HOXC6 in MSI-H and microsatellite-stable (MSS) samples. The results showed that HOXC6 was overexpressed in RCC MSI-H compared with RCC MSS and LCC samples, suggesting a close association between HOXC6 and MSI-H status ($P < 0.001$, Fig. 1A).

Next, we assessed the prognostic value of HOXC6 based on samples from the TCGA and GSE39582 datasets and found that high expression of HOXC6 was significantly associated with a poor clinical outcome in MSI-H CRC (log rank $P = 0.02$, Fig. 1B).

HOXC6 recruits M2 macrophages infiltration by upregulating the cytokine CCL2

To explore whether HOXC6 plays a role in the interaction between tumor cells and immune cells in the CRC tumor microenvironment, we investigated in detail the functional phenotype under HOXC6 regulation. In this context, we compared the overall transcriptome variation between the HOXC6 + (mean RNA-Seq by expectation maximization, RSEM: 133) and HOXC6- groups (mean RSEM: 12). There were 1,226 DEGs identified between the HOXC6 + and HOXC6- groups, and most of DEGs (1,001, 82%) were upregulated in the HOXC6 + group (Fig. 2A). For example, cytokines such as CCL2, CCL5, and IL6 had significantly higher expression levels in the HOXC6 + group (Fig. 2A). Furthermore,

(See figure on next page.)

Fig. 2 HOXC6 was correlated with enhanced cytokine interaction and TME reshuffling. **A** Volcano plot of DEGs identified between the low and high HOXC6 expression groups using TCGA samples. **B** GO enrichment of DEGs in the high HOXC6 expression group using TCGA samples. **C** KEGG pathway enrichment of DEGs in the HOXC6 high-expression group using TCGA samples. **D** Tumor purity, leukocyte fraction, and M2 macrophage infiltration were compared between the HOXC6 high- and low-expression groups. **E** Higher M2 macrophage infiltration was observed in the high HOXC6 expression group than in the low HOXC6 expression group in the ZUCI cohort. **F** Relative mRNA expression of CCL2 in the HOXC6-OE and siHOXC6 groups compared to the NC group in HCT116 cells. **G** ELISA detection of CCL2 concentrations in the HOXC6-OE and siHOXC6 groups compared to the NC group using HCT116 cell supernatants. **H** Representative images of samples with high HOXC6 expression and high M2 macrophage infiltration. **I** Correlation between HOXC6 expression and M2-TAM infiltration in 53 RCC samples from the ZUCI cohort. *: $P < 0.05$; **: $P < 0.01$; ***: $P < 0.001$

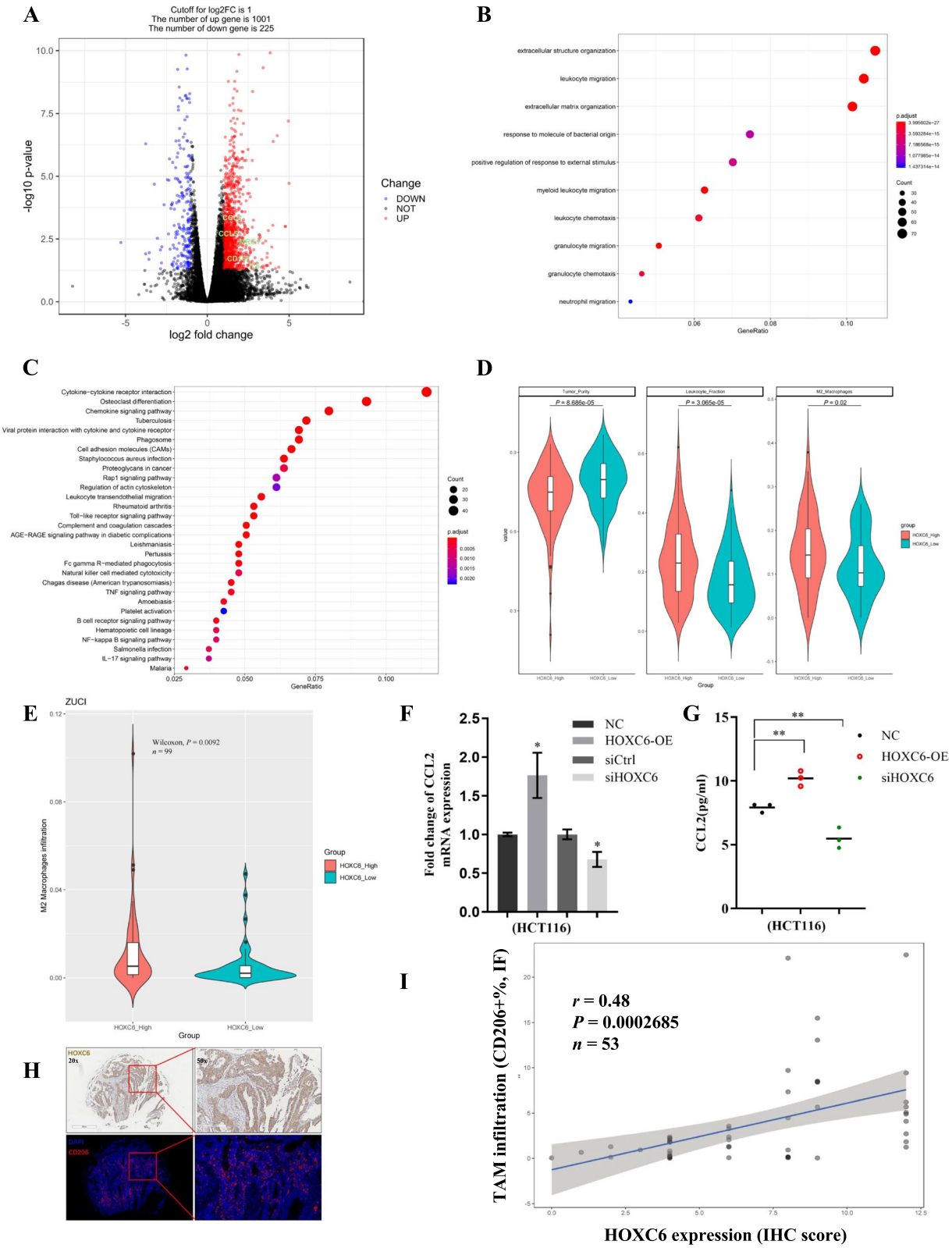

Fig. 2 (See legend on previous page.)

GO enrichment analysis revealed that these upregulated DEGs mainly participate in leukocyte migration ($P<0.001$, FDR adjusted), extracellular matrix organization ($P<0.001$), and leukocyte chemotaxis ($P<0.001$, Fig. 2B). KEGG pathway enrichment analysis showed that cytokine−cytokine receptor interaction ($P<0.001$), osteoclast differentiation ($P<0.001$) and chemokine signaling pathway ($P<0.001$, Fig. 2C) were the top enriched pathways, indicating that high HOXC6 expression is linked to TME remodeling. Thus, tumor purity was compared between the HOXC6+and HOXC6- groups. Not surprisingly, tumor purity was significantly decreased in the HOXC6+group ($P=8.6E-5$, Wilcoxon test, Fig. 2D). To further determine the cell types accounting for the decreased tumor purity in the HOXC6+group, CIBERSORT was used to estimate the abundance of diverse cell types in CRC. We found that the proportion of leukocytes was significantly increased in the HOXC6+group ($P=3.1E-5$, Wilcoxon test, Fig. 2D), and this difference was mainly due to M2 macrophage infiltration ($P=0.02$, Wilcoxon test, Fig. 2D). The increased infiltration of M2 macrophages in the HOXC6+group was also observed in the ZUCI cohort (Fig. 2E). CCL2 was reported as a typical macrophage-attracting cytokine that could recruite M2 macrophages [17]. Therefore, we speculated that M2 macrophages could be recruited into the tumor region by CCL2 upregulation mediated by high HOXC6 expression.

To test this hypothesis, we experimentally investigated the relationship between HOXC6 expression and CCL2/M2 macrophage infiltration. First, we selected the HCT116 cell line for HOXC6-overexpression and knockdown because HCT116 is a dMMR cell line (Fig. S1A and B). At the mRNA level, CCL2 was elevated by 1.8-fold ($P<0.05$, *t* test) in the HCT116 HOXC6-OE group and decreased by 41% ($P<0.05$, *t* test) in the HCT116 siHOXC6 group compared to the NC group (Fig. 2F). At the protein level, the CCL2 concentration in cell culture supernatants was elevated from 7.9 to 10.2 pg/ml ($P<0.01$, *t* test) with HOXC6 overexpression and decreased to 5.1 pg/ml ($P<0.01$, *t* test) with HOXC6 konocdown in HCT116 cells (Fig. 2G). Furthermore, IF analysis was performed for 53 stage II and 47 stage III&IV RCC samples collected from the ZUCI cohort to evaluate M2 macrophage infiltration according to the CD206-positive area (Fig. 2H). Through combined evaluation of HOXC6 and CD206, we confirmed a significant positive correlation between M2 macrophage infiltration and HOXC6 expression ($P<0.05$, Fig. 2I and Fig. S2). We also compared the clinical characteristics between the HOXC6+group and the HOXC6- group based on RNAseq of 99 ZUCI MSI-H fresh frozen samples and found that no significant difference was observed in sex, age, stage, differentiation grade, perineural invasion, vascular invasion and MMR status ($P>0.05$); however, the HOXC6+group had significantly more RCC ($P=0.011$) and less early-onset ($P=0.008$) cases than the HOXC6- group (Table S1).

Crosstalk between HOXC6^{high} tumor cells and M2-TAMs

Next, we explored the detailed molecular mechanism of the crosstalk between HOXC6-overexpressing tumors and M2 macrophages. GSEA was performed to identify prominent signatures associated with high HOXC6 expression. Interestingly, IL6/JAK/STAT3 signaling (normalized enrichment score, NES=1.78, $P=0.014$, Fig. 3A) and EMT (NES=1.71, $P=0.038$, Fig. 3B) were characteristic of HOXC6 overexpression. Considering that HOXC6 is related to M2 macrophage infiltration probably mediated by CCL2 and that cancer cell EMT could be induced by IL6 secreted from TAMs [18], we hypothesized that M2 macrophages induce EMT in tumor cells by regulating the IL6/HOXC6 axis.

A coculture assay was performed to test our hypothesis. M2 macrophages were sequentially induced by PMA, IL4 and IL13 from progenitor THP-1 cells in vitro (Fig. 3C). CD163 and CD206, two M2 macrophage surface markers, were significantly upregulated in induced M2 macrophages compared to THP-1 cells (Fig. 3D). Then, the optimal coculture time for M2 macrophages or cytokine IL6 and tumor cells was determined to be 72 h and 48 h according to the expression levels of HOXC6, respectively (Fig. 3E and F). After 72 h of coculture, the expression of IL6 in M2 macrophages was upregulated threefold compared to that in M2 macrophages alone ($P<0.01$, *t* test, Fig. 3G). Furthermore, both the mRNA levels and

(See figure on next page.)

Fig. 3 Crosstalk between HOXC6.^{high} HCT116 cells and M2-TAMs. **A** and **B** GSEA showed that the IL6/JAK/STAT3 pathway and EMT process were significantly enriched in the HOXC6-overexpressing group. **C** Flow chart of M2 macrophages induced from THP-1 cells and schematic diagram for coculturing of M2 macrophages and tumor cells. **D** Relative mRNA expression of CD163 and CD206 in induced M2 macrophages and THP-1 cells. **E** Protein expression of HOXC6 in HCT116 cells cocultured with M2 macrophages over a time period from 0 to 72 h. **F** Protein expression of HOXC6 in HCT116 cells cocultured with 50 ng/ml IL6 over a time period from 0 to 48 h. **G** Relative mRNA expression of IL6 in M2 macrophages with and without coculture with HCT116 cells. **H** Relative mRNA expression of IL6 in M2 macrophages cocultured with shCtrl, shHOXC6, or HOXC6-OE HCT116 cells. **I** ELISA detection of IL6 concentrations in M2 macrophages cocultured with shCtrl, shHOXC6, and HOXC6-OE HCT116 cells. **J** Protein expression of IL6 in M2 macrophages cocultured with shCtrl, shHOXC6, and HOXC6-OE cells.*: $P<0.05$; **: $P<0.01$; ***: $P<0.001$

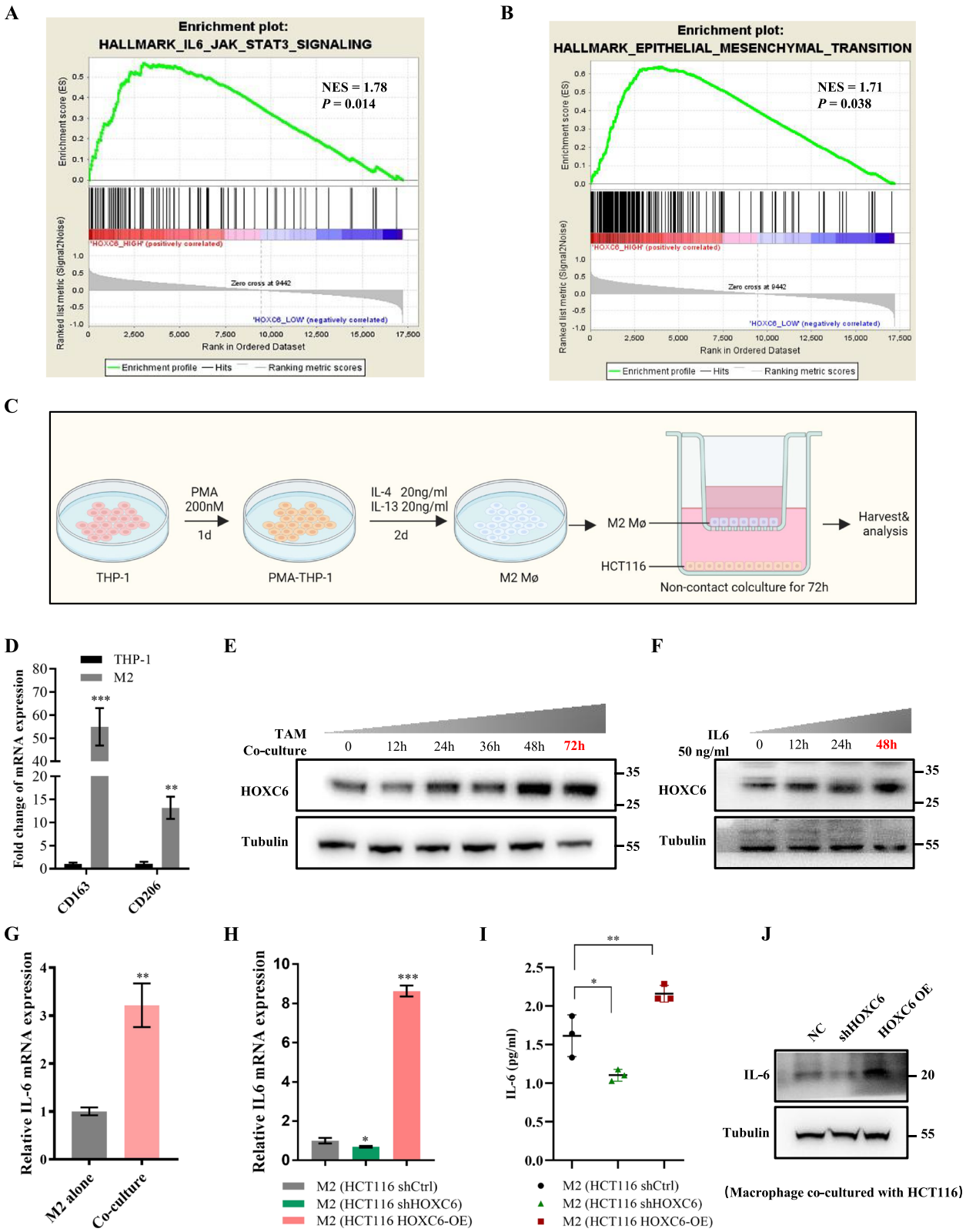

Fig. 3 (See legend on previous page.)

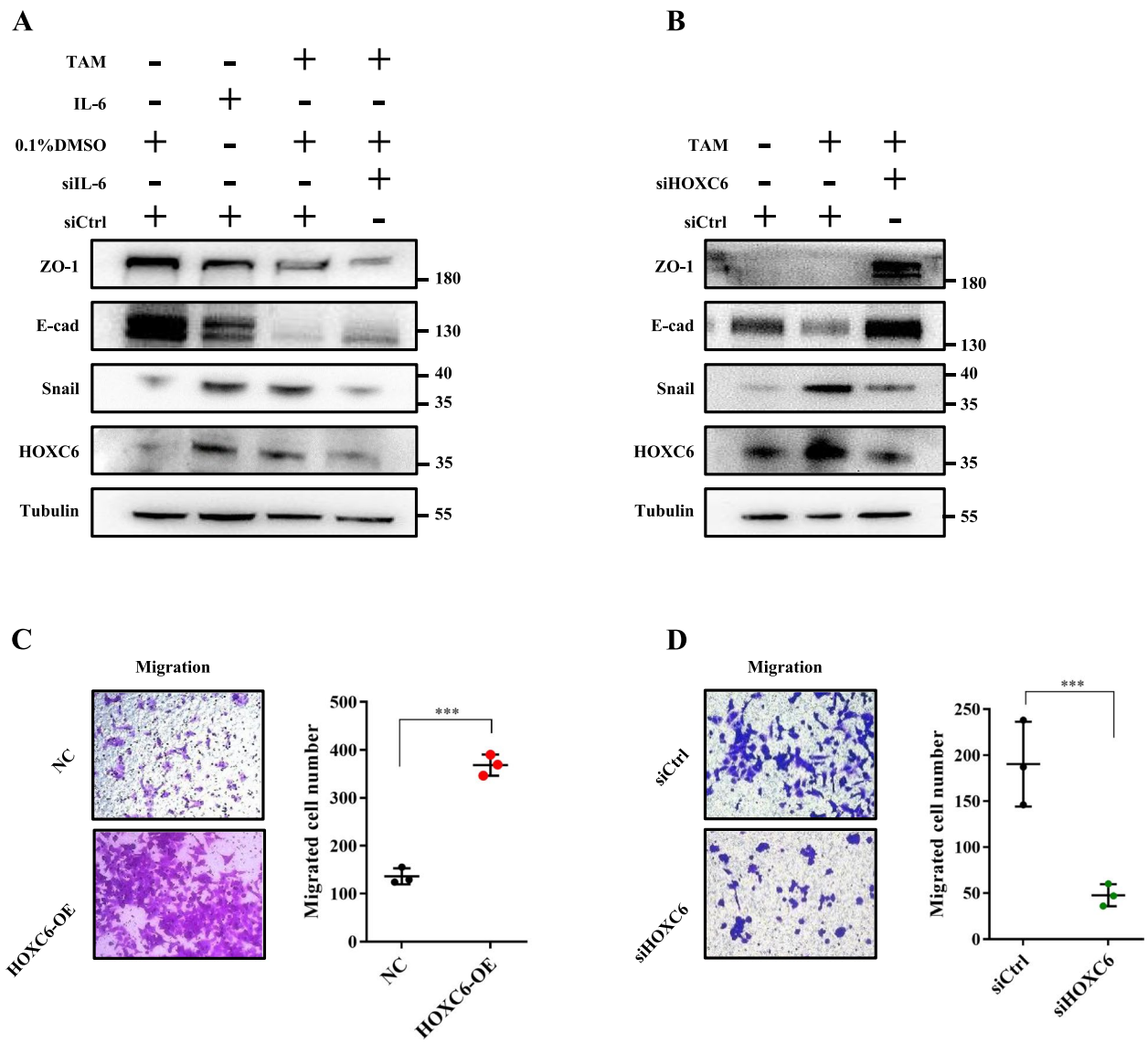

Fig. 4 M2 macrophages induced the EMT of HCT116 by secreting IL6 and regulating the IL6/HOXC6 axis. **A** Protein expression of ZO-1, E-cadherin, snail, and HOXC6 in four different treated HCT116 groups. **B** Protein expression of ZO-1, E-cadherin, Snail, and HOXC6 in three different treated HCT116 groups. **C** Transwell experiments without Matrigel in the NC and HOXC6-OE HCT116 groups. **D** Transwell experiments without Matrigel in siCtrl and siHOXC6 HCT116 groups. ***: $P < 0.001$; n.s.: no significance

protein levels of IL6 (including extracellular secretion) in M2 macrophages were significantly decreased when these cells were cocultured with ltv-shHOXC6 cells and increased when they were cocultured with HOXC6-OE cells compared to shCtrl cells in the HCT116 cell background (Fig. 3H-J).

Next, the influence of M2 macrophages on tumor cells was investigated. Result showed that the canonical markers of epithelium ZO-1 and E-cadherin were downregulated and mesenchyme marker snail was upregulated in HCT116 cells, which occurred during coculture with M2 macrophages; this effect was similar to the effect when human recombinant IL6 was added to the medium (Fig. 4A). In addition, HOXC6 could be upregulated when HCT116 cells were cocultured with M2 macrophages or treated with IL6 only (Fig. 4A). When IL6 was knocked down in M2 macrophages, EMT was reversed and HOXC6 was downregulated (Fig. 4A). In addition, knockdown of HOXC6 in HCT116 cells induced mesenchymal epithelial transition (MET) even when the cells were cocultured with M2 macrophages (Fig. 4B), indicating that HOXC6 plays a critical role in CRC metastasis.

To test our hypothesis, we performed a transwell assay to evaluate whether HOXC6 could enhance the migration ability of tumor cells by inducing EMT. The results showed that the migration ability was greatly enhanced under high expression of HOXC6 (Fig. 4C and D); however, the proliferation ability of tumor cells remained unchanged (Fig. S3A and B).

In summary, high HOXC6 expression in tumor cells can promote secretion of IL6 from M2 macrophages, and in turn, M2 macrophages could induce EMT of tumor cells through the IL6/HOXC6 axis.

M2 macrophages inactivate effector T cell by inhibiting the costimulator 4-1BB

MSI-H tumors commonly have a high neoantigen load and high $CD8^+$ T-cell infiltration and are thus suitable for immune checkpoint blockade (ICB) therapy, which prompted us to investigate the number of neoantigen and $CD8^+$ T-cell infiltration level differences between the HOXC6 + and HOXC6- groups. Notably, no significant difference in $CD8^+$ T-cell infiltration was observed between the HOXC6 + and HOXC6- groups (Fig. S4A and B). Nevertheless, the tumor mutational burden (TMB) (in both TCGA and ZUCI cohorts) and the numbers of single nucleotide variation (SNV)-derived and insertion or deletion (INDEL)-derived neoantigens were abnormally moderately increased in the HOXC6 + group than the HOXC6- group (Fig. S4C-F). We then speculated that the $CD8^+$ T cells may be exhausted or inactivated in the HOXC6 + group despite the numerous tumor-associated antigens. To this end, we detected the expression of canonical T-cell costimulators (CD27, CD28, and 4-1BB) and checkpoints (CTLA-4, LAG3, PD1, TIGIT, and TIM3) using a coculture system consisting of HCT116 cells, M2 macrophages and $CD8^+$ T cells (Fig. 5A). Interestingly, we found that 4-1BB in $CD8^+$ T cells was significantly downregulated (~ 50%) by M2 macrophages (Fig. 5B). To further confirm the regulation axis of high HOXC6 expression, M2 macrophage infiltration and 4-1BB downregulation in T cell in vivo, single cell sequencing of subcutaneous tumor xenograft constructed by mice MC38 HOXC6-OE and HOXC6-NC cells was performed. Notably, high HOXC6 expression can promote M2 macrophage infiltration (Fig. S5A and B). Additionally, T cell 4-1BB was significantly downregulated in the HOXC6-OE group (Fig. S5C and D).

Given that HOXC6 is not a currently approved druggable target, we explored whether inhibiting the IL6/JAK pathway was a potential alternative therapeutic strategy for HOXC6-overexpressing MSI-H CRC. Ruxolitinib, a selective JAK1/2 inhibitor, suppressed HOXC6 and snail expression in tumor cells (Fig. S6A and B) and phosphorylated-STAT3 (p-STAT3) in a dose-dependent manner in M2 macrophages (Fig. 5C). Interestingly, the ruxolitinib has a beneficial effect at low dosage of 1 uM and the expression of 4-1BB was restored almost linearly in $CD8^+$ T cells cocultured with M2 macrophages treated with increasing concentrations (1-50uM) of ruxolitinib (Fig. 5D). Moreover, IFN-γ and TNF-α secretion by $CD8^+$ T cells was also enhanced correspondingly when M2 macrophages were treated with increasing doses of ruxolitinib (3.125, 6.25, 12.5, 25, 50uM), indicating that the cytotoxic effect was recovered despite the presence of macrophages (Fig. 5E and F). Furthermore, we found that monotherapy with ruxolitinib, which affects IL6 levels, had a superior curative effect compared with the PD1 inhibitor toripalimab (45% vs. 10% evaluated by LDH killing test). Toripalimab basically cannot enhance the therapeutic effect when compared with that in the control group. However, the combination of toripalimab and ruxolitinib had additive effects on HOXC6-OE tumor cells, with 60% killing efficiency ($P < 0.01$, Fig. 5G).

To confirm the therapeutic effect of ruxolitinib and PD1 antibody on $HOXC6^{high}$ MSI-H CRC, we performed in vivo efficacy evaluation using human HCT116 cells, M2 macrophages and $CD8^+$ T cells in BALB/c mice (Fig. 6A). In vivo fluorescence imaging was carried out five days before treatment, during treatment and five days after treatment (Fig. 6B), and the therapeutic efficacy was evaluated according to the response evaluation

(See figure on next page.)

Fig. 5 M2-TAMs inhibition of effector T cell activation by downregulating 4-1BB. **A** Schematic diagram of noncontact coculture of two or three different cell types. **B** The relative expression levels of costimulators (CD27, CD28, and 4-1BB) and immune checkpoints (CTLA4, LAG3, PD1, TIGIT, and TIM3) in T cells based on the coculture of $CD8^+$ T cells with or without M2 macrophages. **C** Ruxolitinib downregulated the protein expression of phosphorylated STAT3 (p-STAT3) in a dose-dependent manner in M2 macrophages. However, STAT3 was not affected by ruxolitinib. **D** The expression of 4-1BB was upregulated in a dose-dependent manner when $CD8^+$ T cells were cocultured with M2 macrophages treated with ruxolitinib. **E** TNF-α secreted by $CD8^+$ T cells was enhanced when M2 macrophages were treated with ruxolitinib in a dose-dependent manner. **F** IFN-γ secreted by $CD8^+$ T cells in the culture supernatant, as estimated by ELISA, was enhanced when M2 macrophages were treated with ruxolitinib in a dose-dependent manner. **G** Ruxolitinib had a curative effect superior to that of toripalimab in HOXC6-OE HCT116 cells. No benefit was obtained by toripalimab monotherapy. However, doublet therapy with toripalimab (5 μg/ml) and ruxolitinib (12.5 uM) had additive effects on HOXC6-OE tumor cells with 60% killing efficiency, similar to the killing efficiency of the single drug ruxolitinib at 25 uM. The cytotoxic effect of $CD8.^+$ T cells was assessed by LDH assay. *: $P < 0.05$; **: $P < 0.01$; ***: $P < 0.001$

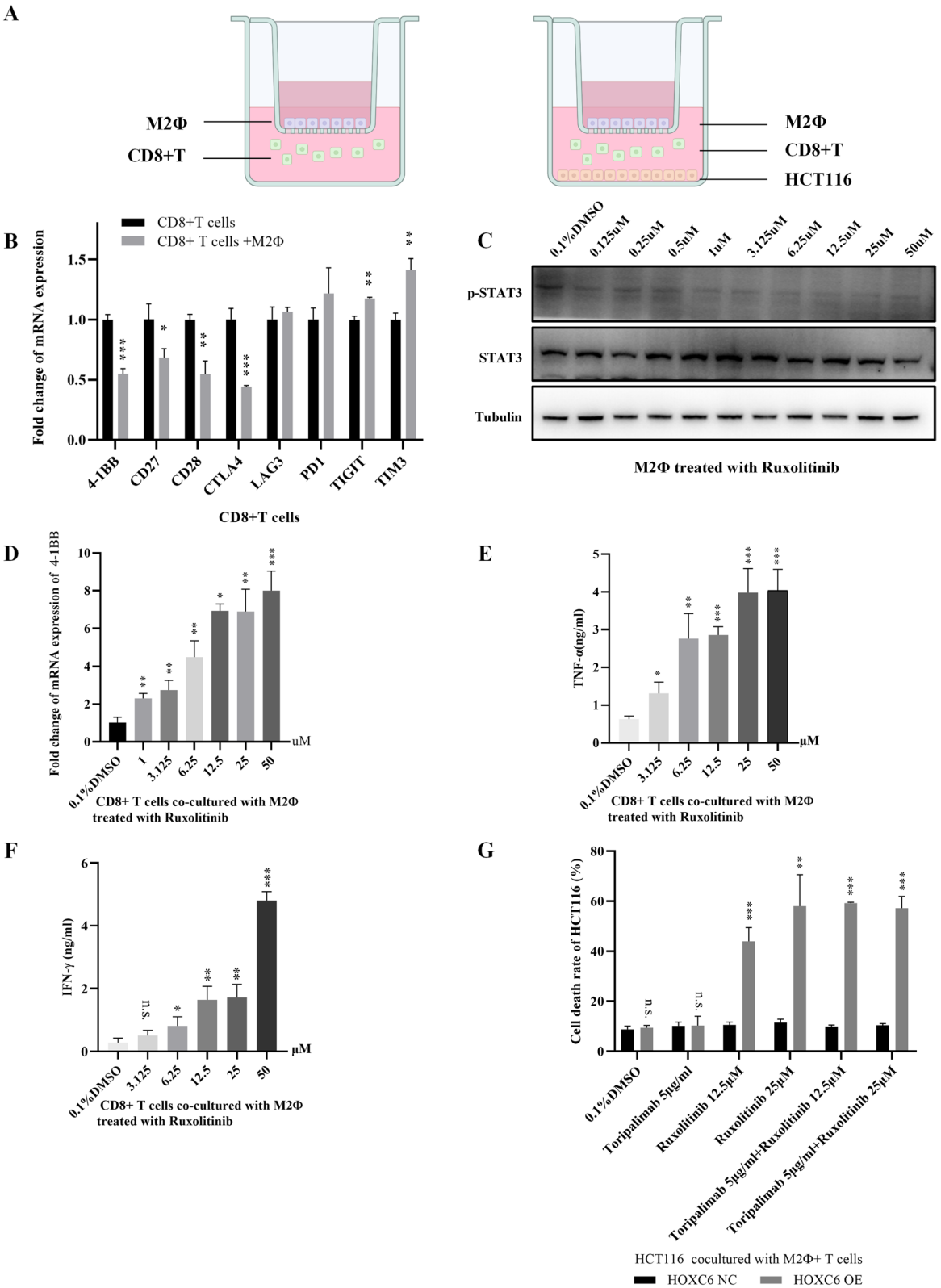

Fig. 5 (See legend on previous page.)

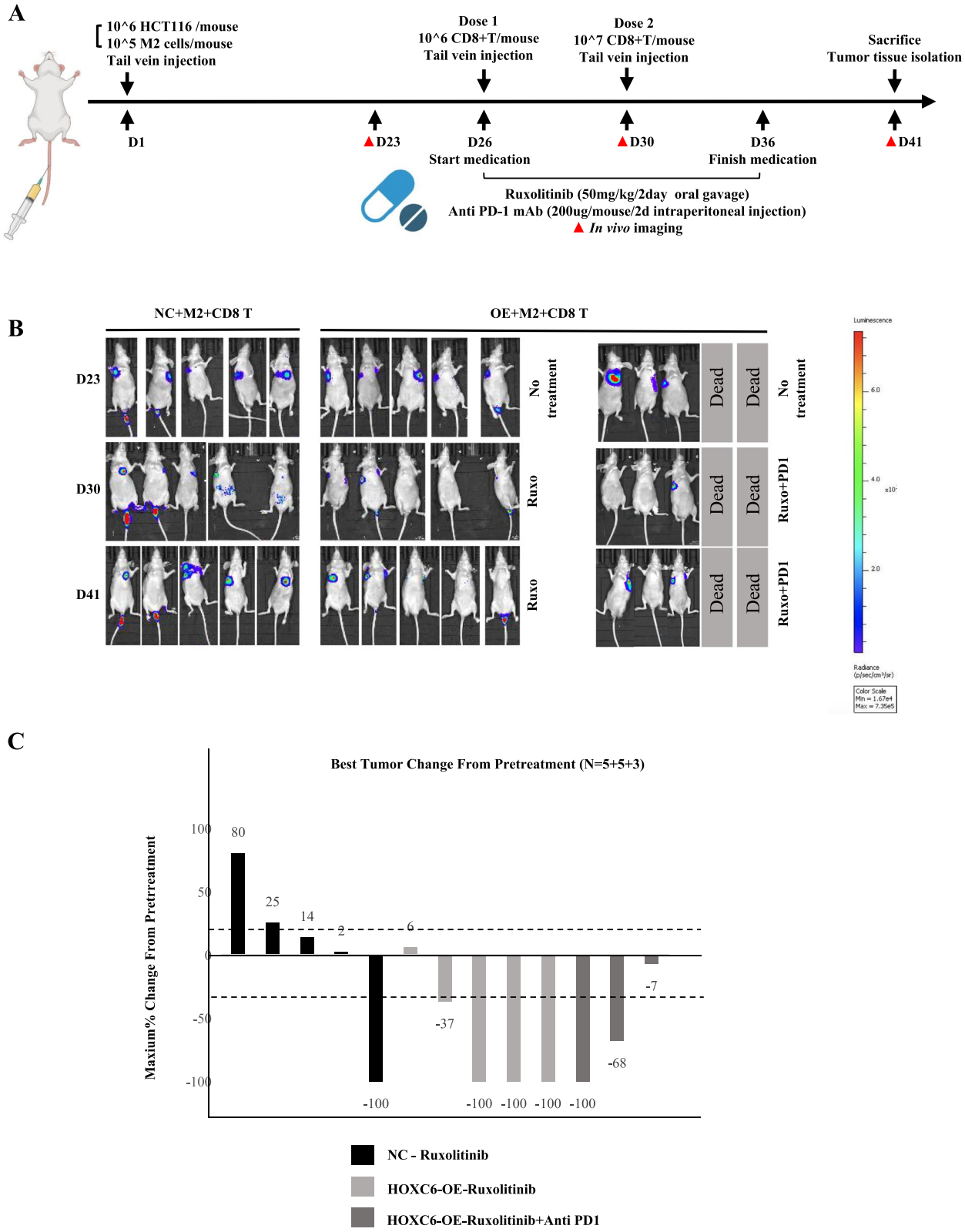

Fig. 6 Ruxolitinib had a better curative effect in the HOXC6-OE group than in the NC group. **A** Schematic diagram of simple humanized immune system construction using $CD8^+$ T cells induced from healthy donor PBMCs. A metastasis model was constructed via tail vein injection of HCT116 cells and M2-TAMs. **B** In vivo imaging of BALB/c nude mice 5 days before treatment, during treatment and 5 days after treatment. **C** Waterfall curve of 12 mice from the NC and HOXC6-OE groups treated with ruxolitinib alone, PD1 antibody alone or combined treatment

criteria in solid tumours (RECIST) standard; the longest diameter of the lung metastases was measured before and after treatment (Fig. 6C). Consistent with the in vitro results, ruxolitinib had a significant inhibitory effect on lung metastasis in the $HCT116^{HOXC6-OE}$ group compared to the $HCT116^{NC}$ group, and the combination of ruxolitinib and an anti-PD1 monoclonal antibody also showed good control of lung metastasis in the $HCT116^{HOXC6-OE}$ group. However, the efficacy of ruxolitinib alone and in combination with ICB remains to be assessed using animal experiments with larger sample sizes.

These results indicated that blockade of the IL6/HOXC6 axis is a promising feasible therapeutic strategy for $HOXC6^{high}$ MSI-H CRC patients.

Discussion

MSI-H tumors generally have a large number of nonsilent mutations (nonsynonymous, indel frameshift, nonsense, and splice site mutations), leading to an increased number of neoepitopes and cytotoxic T lymphocytes (CTLs); thus, they are termed 'hot' tumors [19]. This is one of the important reasons why a high TMB in patients predicts a good clinical response to ICB and prolonged overall survival (OS) [20]. Nevertheless, in this study, higher TMB and neoantigen load in the $HOXC6^{high}$ group were associated with a poor prognosis, and regular anti-PD1 toripalimab therapy was ineffective against HOXC6-OE tumor cells, indicating that MSI-H tumors, as heterogeneous entities [8], are much more complicated than previously thought [15]. Deconvolution of cellular components in tumor tissue revealed significant enrichment of M2 macrophages in the $HOXC6^{high}$ group of MSI-H CRCs. TAMs are the main type of infiltrated immune cell in the TME [21] and have been shown to play an important role in tumorigenesis [22], angiogenesis [23, 24], metastasis [25, 26], and chemoresistance [27–32].

Here, we first reported the mechanisms that contribute to worse clinical outcomes and promising therapeutic strategies for $HOXC6^{high}$ MSI-H CRCs. We found that the cytokine CCL2, which is known to strongly attract macrophages to the tumor region, could be upregulated by HOXC6. IL6 was upregulated in M2-TAMs by coculture with HOXC6-OE CRC cells and vice versa. IL6 secreted by macrophages was associated with EMT of tumor cells, which was consistent with a previous study [18]. EMT has been shown to be closely associated with cancer immunoevasion and immunosuppression [33, 34]. Here, we also found that in addition to reciprocal interactions between CRC and macrophages, M2 macrophages suppress effector T cells by downregulating 4-1BB instead of upregulating checkpoints such as PD1 or LAG3, which may partly explain why more than 50% of MSI-H patients do not respond well to anti-PD1 therapy. Cancer cells with mesenchymal phenotypes are less susceptible to attack by $CD8^+$ T or natural killer (NK) cells [33, 35]. Thus, therapeutic regimens designed to reverse EMT may render cancer more susceptible to immunotherapy.

Based on the mechanisms we explored, the IL6/JAK pathway inhibitor ruxolitinib was utilized to reverse EMT in CRC cells, inhibit the IL6/JAK/STAT3 pathway in M2-TAMs, restore 4-1BB expression in T cells and demonstrated high cytotoxicity against $HOXC6^{high}$ HCT116 cells. Additionally, the combination of ruxolitinib and toripalimab (an anti-PD1 antibody) enhanced the antitumor effect on $HOXC6^{high}$ tumor cells. This synergistic effect can potentially reduce the drug toxicity of ruxolitinib, which highlights the supporting role of ICB in cancer treatment even though no curative effect was observed with ICB alone. Because there is currently no HOXC6-targeted drug and the 4-1BB agonist urelumab (BMS-663513) presents hepatotoxicity, targeting IL6/IL6R or JAK is a feasible strategy for $HOXC6^{high}$ or M2-TAM-high CRCs; related inhibitors include sarilumab (IL6R inhibitor), which was approved by the FDA for Castleman syndrome treatment [36], and ruxolitinib (JAK1/2inhibitor), which was approved by the FDA for myelofibrosis in 2011 [37].

It must be pointed out that some limitations of our study require further research. Firstly, some conclusion of our study was derived from in vitro cell coculture, so we cannot exclude other cells within TME that will disturb the observed relationships. Future work may employ organoid or patient-derived xenografts (PDX) to avoid idealistic experimental design. Second, the molecular mechanism of HOXC6 upregulating CCL2 needs further investigation. Additionally, the pathway of M2 macrophages inactivates T cell should also be clarified in future work.

Conclusion

In conclusion, we identified that $HOXC6^{high}$ MSI-H CRC cells induce exhaustion of $CD8^+$ T cells by interacting with M2 macrophages, which is a novel crosstalk mechanism. In addition, blockade of the IL6/JAK pathway provides an alternative therapeutic strategy to restore $CD8^+$ T-cell cytotoxicity by indirectly targeting $HOXC6^{high}$ tumor cells and M2-TAMs. Consequently, HOXC6 could serve as a biomarker for MSI-H CRC prognosis and a potential therapeutic target for anti-PD1 resistant MSI-H CRC patients.

Abbreviations

CCK8	Cell counting kit-8
CRC	Colorectal cancer
DEGs	Differentially expressed genes
EMT	Epithelial-mesenchymal transition
FDR	False discovery rate

GEO	Gene Expression Omnibus
GO	Gene ontology
GSEA	Gene set enrichment analysis
KEGG	Kyotoencyclopedia of genes and genomes
LCC	Left-sided colon cancer
MSI-H	Microsatellite instability-high
MSS	Microsatellite stable
RCC	Right-sided colon cancer
TCGA	The Cancer Genome Atlas
TME	Tumor microenvironment
TAM	Tumor associated macrophage
ZUCI	Zhejiang University Cancer Institute

Supplementary Information

The online version contains supplementary material available at https://doi.org/10.1186/s12964-025-02167-2.

Supplementary Material 1.

Acknowledgements
Not applicable.

Authors' contributions
LNQ, WXH and SZ designed the study. WXH performed GO, KEGG, and GSEA analysis. LNQ and KLX performed western blots. LNQ performed qRT-PCR, CCK8, Transwell, and ELISA. BTZ, KLW and JNC performed mouse experiments. BTZ collected the human tissue samples. WXH performed the IHC and IF assays. JNC and YMY performed statistical analysis. LNQ, BTZ and WXH wrote the manuscript. All authors read and approved the final manuscript.

Funding
This work was supported by National Natural Science Foundation of China (grant number: 81802883) and Fundamental Research Funds for the Central Universities (grant number: 226–2024-00062) to WXH.

Data availability
No datasets were generated or analysed during the current study.

Declarations

Ethics approval and consent to participate
This study was approved by the Ethics Committee of the Second Affiliated Hospital, Zhejiang University School of Medicine.

Consent for publication
All authors read and are consent for the publication of this manuscript.

Competing interests
The authors declare no competing interests.

Received: 16 September 2024 Accepted: 21 March 2025
Published online: 04 April 2025

References

1. Andre T, et al. Pembrolizumab in Microsatellite-Instability-High Advanced Colorectal Cancer. N Engl J Med. 2020;383(23):2207–18.
2. Ganesh K, et al. Immunotherapy in colorectal cancer: rationale, challenges and potential. Nat Rev Gastroenterol Hepatol. 2019;16(6):361–75.
3. Hu W, et al. Subtyping of microsatellite instability-high colorectal cancer. Cell Commun Signal. 2019;17(1):79.
4. Yang Y, et al. Heterogeneity of MSI-H gastric cancer identifies a subtype with worse survival. J Med Genet. 2021;58(1):12–9.
5. Qi L, et al. HomeoboxC6 promotes metastasis by orchestrating the DKK1/Wnt/beta-catenin axis in right-sided colon cancer. Cell Death Dis. 2021;12(4):337.
6. Imai K, Yamamoto H. Carcinogenesis and microsatellite instability: the interrelationship between genetics and epigenetics. Carcinogenesis. 2008;29(4):673–80.
7. Mootha VK, et al. PGC-1alpha-responsive genes involved in oxidative phosphorylation are coordinately downregulated in human diabetes. Nat Genet. 2003;34(3):267–73.
8. Van den Eynde M, et al. The Link between the Multiverse of Immune Microenvironments in Metastases and the Survival of Colorectal Cancer Patients. Cancer Cell. 2018;34(6):1012-1026.e3.
9. Yu G, et al. clusterProfiler: an R package for comparing biological themes among gene clusters. OMICS. 2012;16(5):284–7.
10. Subramanian A, et al. Gene set enrichment analysis: a knowledge-based approach for interpreting genome-wide expression profiles. Proc Natl Acad Sci U S A. 2005;102(43):15545–50.
11. Newman AM, et al. Robust enumeration of cell subsets from tissue expression profiles. Nat Methods. 2015;12(5):453–7.
12. Aran D, Sirota M, Butte AJ. Systematic pan-cancer analysis of tumour purity. Nat Commun. 2015;6:8971.
13. Wang C, et al. Adoptive antitumor immunotherapy in vitro and in vivo using genetically activated erbB2-specific T cells. J Immunother. 2014;37(7):351–9.
14. Ge W, et al. High-risk stage III colon cancer patients identified by a novel 5-gene mutational signature are characterized by up-regulation of IL-23A and gut bacterial translocation of the tumor microenvironment. Int J Cancer. 2019;146(7):2027–35.
15. Hu W, et al. Hypermutated tumours across 11 cancer types show three distinct immune subtypes. Eur J Cancer. 2021;148:230–8.
16. Hao Y, et al. Dictionary learning for integrative, multimodal and scalable single-cell analysis. Nat Biotechnol. 2024;42(2):293–304.
17. Wang X, et al. HMGA2 facilitates colorectal cancer progression via STAT3-mediated tumor-associated macrophage recruitment. Theranostics. 2022;12(2):963–75.
18. Wei C, et al. Crosstalk between cancer cells and tumor associated macrophages is required for mesenchymal circulating tumor cell-mediated colorectal cancer metastasis. Mol Cancer. 2019;18(1):64.
19. Binnewies M, et al. Understanding the tumor immune microenvironment (TIME) for effective therapy. Nat Med. 2018;24(5):541–50.
20. Samstein RM, et al. Tumor mutational load predicts survival after immunotherapy across multiple cancer types. Nat Genet. 2019;51(2):202–6.
21. Morrison C. Immuno-oncologists eye up macrophage targets. Nat Rev Drug Discov. 2016;15(6):373–4.
22. Schwitalla S, et al. Intestinal tumorigenesis initiated by dedifferentiation and acquisition of stem-cell-like properties. Cell. 2013;152(1–2):25–38.
23. Murdoch C, et al. The role of myeloid cells in the promotion of tumour angiogenesis. Nat Rev Cancer. 2008;8(8):618–31.
24. Valkovic T, et al. Correlation between vascular endothelial growth factor, angiogenesis, and tumor-associated macrophages in invasive ductal breast carcinoma. Virchows Arch. 2002;440(6):583–8.
25. Pollard JW. Tumour-educated macrophages promote tumour progression and metastasis. Nat Rev Cancer. 2004;4(1):71–8.
26. Fan QM, et al. Tumor-associated macrophages promote cancer stem cell-like properties via transforming growth factor-beta1-induced epithelial-mesenchymal transition in hepatocellular carcinoma. Cancer Lett. 2014;352(2):160–8.
27. Yang J, et al. Tumor-associated macrophages regulate murine breast cancer stem cells through a novel paracrine EGFR/Stat3/Sox-2 signaling pathway. Stem Cells. 2013;31(2):248–58.
28. Dijkgraaf EM, et al. Chemotherapy alters monocyte differentiation to favor generation of cancer-supporting M2 macrophages in the tumor microenvironment. Cancer Res. 2013;73(8):2480–92.
29. Mantovani A, Allavena P. The interaction of anticancer therapies with tumor-associated macrophages. J Exp Med. 2015;212(4):435–45.
30. Shojaei F, et al. Tumor refractoriness to anti-VEGF treatment is mediated by CD11b+Gr1+ myeloid cells. Nat Biotechnol. 2007;25(8):911–20.
31. Shree T, et al. Macrophages and cathepsin proteases blunt chemotherapeutic response in breast cancer. Genes Dev. 2011;25(23):2465–79.
32. Paulus P, et al. Colony-stimulating factor-1 antibody reverses chemoresistance in human MCF-7 breast cancer xenografts. Cancer Res. 2006;66(8):4349–56.
33. Jiang Y, Zhan H. Communication between EMT and PD-L1 signaling: New insights into tumor immune evasion. Cancer Lett. 2020;468:72–81.

34. Wang L, et al. EMT- and stroma-related gene expression and resistance to PD-1 blockade in urothelial cancer. Nat Commun. 2018;9(1):3503.
35. Dongre A, et al. Epithelial-to-Mesenchymal Transition Contributes to Immunosuppression in Breast Carcinomas. Cancer Res. 2017;77(15):3982–9.
36. Ascierto PA, et al. Insights from immuno-oncology: the Society for Immunotherapy of Cancer Statement on access to IL-6-targeting therapies for COVID-19. J Immunother Cancer. 2020;8(1):e000878.
37. FDA, https://www.accessdata.fda.gov/drugsatfda_docs/label/2011/202192lbl.pdf. 2011.

Publisher's Note